A note on ^{10}Be-derived mean erosion rates in catchments with heterogeneous lithology. Examples from the western Central Andes.

May 28, 2015

S. Carretier[1,2,3], V. Regard[3,1,2], R. Vassallo[4,5,6], J. Martinod[4,5,6], F. Christophoul[3,1,2], E. Gayer[10], L. Audin[7,8,9], and C. Lagane[1,2,3]

[1] IRD, UR 234, GET, 14 avenue E. Belin, F-31400, Toulouse, France
[2] CNRS, GET, 14 avenue E. Belin, F-31400, Toulouse, France
[3] Université de Toulouse, UPS, GET, 14 avenue E. Belin, F-31400 Toulouse, France
[4] Université de Savoie, ISTerre, F-73376 Le Bourget du Lac, France
[5] CNRS, ISTerre, F-73376 Le Bourget du Lac, France
[6] IRD, ISTerre, F-73376 Le Bourget du Lac, France
[7] IRD, ISTerre, Grenoble, France
[8] Université de Grenoble, ISTerre, Grenoble, France.
[9] CNRS, ISTerre, Grenoble, France.
[10] Institut de Physique du Globe de Paris, Sorbonne Paris Cité, Univ Paris Diderot, UMR 7154 CNRS, F-75005 Paris, France

This article has been accepted for publication and undergone full peer review but has not been through the copyediting, typesetting, pagination and proofreading process, which may lead to differences between this version and the Version of Record. Please cite this article as doi: 10.1002/esp.3748

Abstract

Millennial catchment-mean erosion rates derived from terrestrial cosmogenic nuclides (TCN) are generally based on the assumption that the lithologies of the parent rock each contain the same proportion of quartz. This is not always true for large catchments, in particular at the edge of mountainous plateaus where quartz-rich basement rocks may adjoin sedimentary or volcano-sedimentary rocks with low quartz content. The western Central Andes is an example of this type of situation. Different quartz contents may be taken into account by weighting the TCN production rates in the catchment. We recall the underlying theory and show that weighting the TCN production rate may also lead to bias in the case of a spatial correlation between erosion rate and lithology. We illustrate the difference between weighted and unweighted erosion rates for seven catchments (16 samples) in southern Perú and northern Chile and show variations up to a factor of 2 between both approaches. In this dataset, calculated erosion rates considering only granitoid outcrops are better correlated with catchment mean slopes than those obtained without taking into account the geological heterogeneity of the drained watershed. This dataset analysis demonstrates that weighting erosion rates by relative proportions of quartz is necessary to evaluate the uncertainties for calculated catchment-mean erosion rates and may reveal the correlation with geomorphic parameters.

Introduction

Since the pioneer works of *Brown et al.* (1995) and *Granger et al.* (1996), the use of Terrestrial Cosmogenic Nuclides (TCNs) to calculate the catchment mean denudation rate has revolutionized geomorphology (e.g. *von Blanckenburg*, 2005). The method is based on the assumption that there is a secular equilibrium between the production of TCN and the loss by erosion (and radioactive decay for unstable isotopes) everywhere within a catchment, such that the mean TCN concentration of the river sediment is inversely proportional to the mean denudation rate of the catchment upstream. The TCN concentration of river sediment is measured in selected minerals, such as quartz for ^{10}Be. Consequently, it must be additionally assumed that the proportion of quartz is the same in all eroding parent rocks, such that the quartz and material outfluxes are proportional.

A problem arises if the catchment is composed of lithologies with different quartz content, either naturally (*Schaller et al.*, 2001) or because dissolution has concentrated the quartz at the soil surface (*Small et al.*, 1999). Lithological

variation is common in catchments larger than several tens of km^2. In magmatic arc such as the Andes for example, volcanic rocks with small amounts of quartz adjoin quartz-rich granitic terranes (e.g. *Kober et al.*, 2009). In this case, the relative contribution of each lithology to the quartz outflux does not only depend on its erosion rate and on the local TCN production rate, but also on its quartz content. As an example, let us consider a granite with 25% of quartz eroding very slowly (high TCN concentration) adjoining a volcano-detritic rock with 2 % of quartz eroding very fast (low TCN concentration). If the quartz content is not taken into account, the TCN contribution of the volcano-detritic rock will be incorrectly interpreted as reflecting a low denudation rate, and thus the catchment denudation rate will also be underestimated. This problem may be critical when comparing catchments along a mountain range with a heterogeneous lithology distribution.

A continuous debate has focused on the relative weight of different denudation factors such as mean slope, river steepness, lithology or precipitation rate. If the lithological variations are not considered, this could affect the correlation between the calculated denudation rates and these factors, and might partly explain why the mean slope, for example, is not always shown as controlling the denudation rate (e.g. *Insel et al.*, 2010; *Norton et al.*, 2011; *Hippe et al.*, 2012). In order to limit this bias, TCN production rates have been weighted by the relative quartz content of each lithology (e.g. *Safran et al.*, 2005; *Aguilar et al.*, 2014; *Carretier et al.*, 2013). However, the theoretical basis of this approach has not yet been described in detail.

In this paper, we analyse the basis and the consequence of this approach for the calculated denudation rates. We first recall the underlying theory and then we illustrate different situations using large catchments in southern Peru draining the central Andes. We present 14 new ^{10}Be data and use 2 ^{10}Be data from *Carretier et al.* (2015). These catchments deeply incise the Andean forearc in response to surface uplift that began before ~8 Ma (*Thouret et al.*, 2007; *Schildgen et al.*, 2009, 2010). This evolution has progressively exhumed different lithologies during the propagation of erosion upstream. This is a typical situation for a transient topography responding to uplift, which can be generalized to other mountain ranges.

Theory

We recall here the theory (*Brown et al.*, 1995; *Granger et al.*, 1996; *Bierman and Steig*, 1996; *von Blanckenburg*, 2005), emphasising the proportion of the selected mineral (we use quartz here) in the parent lithology. We do not account for the radioactive decay and only consider spallation for a comparison with the initial derivation of *Brown et al.* (1995) and *Granger et al.* (1996). We also ignore variations in rock density associated with different lithologies. Chemical weathering is not considered (*Riebe and Granger*, 2013). Thus we use the term

erosion and not denudation in the following. These simplifications are further discussed below. The variables used in the following equations are defined in Table 1.

The mean TCN concentration of river sediment gathered at the catchment outlet N is the ratio of the TCN outflux to the quartz outflux:

$$N = \frac{\Psi_c}{\Psi_q} \tag{1}$$

Each flux is expressed as:

$$\Psi_c = \sum_1^n N_i \rho \epsilon_i \chi_i \, dx^2 \tag{2}$$

and

$$\Psi_q = \sum_1^n \rho \epsilon_i \chi_i \, dx^2 \tag{3}$$

where the sum applies to the pixels of a catchment DEM. This method assumes that the TCN concentration has reached a steady state everywhere within the catchment, such that, if we only consider one particle and no radioactive decay,

$$N_i \epsilon_i = \mu P_i \tag{4}$$

Ψ_c then becomes:

$$\Psi_c = \sum_1^n \mu P_i \chi_i \, dx^2 \tag{5}$$

yielding an expression of N:

$$N = \frac{\sum_1^n \mu P_i \chi_i}{\sum_1^n \epsilon_i \chi_i} \tag{6}$$

Dividing both denominator and numerator by the sum of the quartz fractions, we obtain

$$N = \mu \frac{\sum_1^n P_i \chi_i / \sum_1^n \chi_i}{\sum_1^n \epsilon_i \chi_i / \sum_1^n \chi_i} \tag{7}$$

$$= \frac{\mu \, P_w}{\sum_1^n \epsilon_i \chi_i / \sum_1^n \chi_i} \tag{8}$$

In the numerator of N, $P_w = \sum_1^n P_i\chi_i / \sum_1^n \chi_i$ is the catchment-mean production rate weighted by the proportion of quartz, and has been used by several authors to take into account the quartz content of the parent rocks (e.g. *Safran et al.*, 2005).

Now, we define a weighted mean erosion rate ϵ_w as the ratio between the quartz flux Ψ_q divided by the catchment area $n\,dx^2$, and weighted by the mean fraction of quartz in the parent lithologies χ ($= \frac{1}{n}\sum_1^n \chi_i$) and the quartz density:

$$\epsilon_w = \frac{1}{\chi}\frac{1}{\rho}\frac{\Psi_q}{n\,dx^2} \tag{9}$$

It can be proven that ϵ_w is the denominator of N in equation 8:

$$\epsilon_w = \frac{\sum_1^n \epsilon_i\chi_i}{\sum_1^n \chi_i} \tag{10}$$

Inserting equation 9 into equation 8 leads to a similar form of the original model provided by *Brown et al.* (1995) and *Granger et al.* (1996) where the averaged TCN production rate for the catchment is replaced by the weighted mean TCN production rate P_w:

$$\epsilon_w = \frac{\mu P_w}{N} \tag{11}$$

This original model was constructed following the same reasoning but assuming that the quartz content is homogenous and can be written as

$$\epsilon_u = \frac{\mu P_u}{N} \tag{12}$$

where ϵ_u and P_u stand for the unweighted erosion rate and the TCN production rate, respectively.

However, there is a problem because the true mean catchment-mean erosion rate ϵ is usually defined as the average of the local erosion rates

$$\epsilon = \frac{1}{n}\sum_1^n \epsilon_i \tag{13}$$

and ϵ_w defined by equation 9 is not equal (neither ϵ_u) to ϵ, except for the obvious case where χ_i is homogeneous.

For instance, consider a relatively gentle catchment (homogeneous P) composed of three patches of equal areas eroding at rates of 1, 2, and 3 erosion units. These patches have different lithologies with quartz fractions of 1, 5 and

20 percent, respectively. In this case, $\epsilon_w = 3.4$, while $\epsilon = 2$ erosion units. Also in this case, ϵ_u is 3.4. The ϵ_u and ϵ_w values would be different if the different lithologies were spread out at different elevations. In fact, the mean ^{10}Be production rate would be calculated differently, either considering P_u or P_w. In order to compare the departure of ϵ_w and ϵ_u from the true erosion rate value ϵ, we take the previous example further. We now consider that χ_i, ϵ and P are different for the three lithological patches. The different P means that the patches are located at different elevations (Figure 1). The mean ^{10}Be concentration that could be measured at this theoretical catchment outlet is obtained by using Equation 1. The mean ^{10}Be production rate P_u is calculated by simply averaging the ^{10}Be production rates. From these two values, we deduce ϵ_u using Equation 12. In order to calculate ϵ_w we use Equation 11. Then we vary χ_i, P_i and ϵ_i for the three areas by permuting the values indicated in Figure 1 (these values are different in the three areas), yielding different ϵ_u and ϵ_w values for the whole catchment.

Figure 1 shows that both ϵ_u and ϵ_w are different from ϵ. The range of ϵ_w (between 0.5 and 1.5 times the true value) is smaller than ϵ_u (between 0.25 and 2.5 times the true value). For both ϵ_w and ϵ_u, the largest overestimation of ϵ occurs when the erosion rate is locally correlated with the proportion of quartz. The largest underestimation occurs when the erosion is inversely correlated with the proportion of quartz. However, these biases are lower for ϵ_w in both cases, because the weighting used to calculate P_w decreases this bias. The ratio of ϵ_u/ϵ_w varies between 0.6 and 1.5. The largest ϵ_u/ϵ_w values occurs when the highest quartz content is found at the lower (^{10}Be production rate) elevation, the smallest ϵ_u/ϵ_w value arises when the highest quartz content is found at the highest elevation.

For catchments in which the lithology and the erosion rate are correlated or inversely correlated, both strategies (calculating ϵ_w or ϵ_u) are likely to yield a significant bias with regards to the mean erosion rate. In the next section, we show how the calculated mean erosion rate is changed by either considering or not the quartz content for several catchments in the western Central Andes characterised by lithological contrasts.

Application to catchments in the western central Andes

Study area

The forearc of the Andes in southwest Peru and northern Chile, from the coast to the Altiplano plateau, is composed of a coastal scarp reaching 700 m on average, a low relief Coastal Cordillera with an elevation between 500 and 1000 m, a Pampa surface dipping 2-4^o to the west, and the main Cordillera reaching

a mean elevation of ∼4000 m at the margin of the Altiplano plateau. The main river catchments are comprised of deep canyons cutting into the Pampa surface and a more dentritic drainage network in the main Cordillera. The climate is dry with precipitation rates lower than 200 mm/yr at low elevations, whereas catchment heads on the Altiplano plateau receive more precipitation due to the easterly winds. During the El Niño period, precipitation from the Pacific westerly winds increase on the coast (*Garreaud et al.*, 2009).

The age of the forearc and western Cordillera elevations is a matter of debate, but a significant regional surface uplift (∼ 1000-2000 m) has occurred since 25 Ma, and possibly 9 Ma (*Farías et al.*, 2005; *Garzione et al.*, 2006; *Sempere et al.*, 2006; *Thouret et al.*, 2007; *Hoke et al.*, 2007; *Schildgen et al.*, 2007; *Garzione et al.*, 2008; *Barnes and Ehlers*, 2009; *Schildgen et al.*, 2009, 2010; *Garcia et al.*, 2011). This surface uplift has generated deep incision of canyons and increased the erosion in the catchments draining the Altiplano plateau. River profiles show knick-points of several hundreds of meters, showing that the overall topography is transient (*Garcia and Hérail*, 2005; *Schildgen et al.*, 2009; *Jeffery et al.*, 2013).

Previous works on erosion in this area

As we are interested in measuring the effect of "lithological" bias affecting regional variations in erosion rates, in this subsection we briefly review previous works on erosion rates in this region. *Abbuehl et al.* (2010, 2011a,b) obtained ^{10}Be-derived catchment erosion rates in the Rio Piura (5^oS), Rio Pisco (13^oS) and Rio Lluta (18^oS) between 0.01 mm/yr (Altiplano) to 0.25 mm/yr (bottom edge of the Andean scarp). *Carretier et al.* (2015) provided ^{10}Be-derived catchment erosion rates at two sampling points in the Cañete catchment (13^oS) and Oconã catchment (16^oS). The values are ∼0.05 mm/yr and ∼0.15 mm/yr, respectively, but significantly depend on the use of P_u or P_w to calculate the erosion rate. These two samples are included in the present paper (Table 2). At these two sample sites, *Carretier et al.* (2015) also analysed the mean ^{10}Be concentrations of granitoid pebbles. They obtained ^{10}Be concentrations that were more than ten times lower for these pebbles. Granitoid hypsometry cannot explain this difference, thereby suggesting that the granitoid pebbles were derived from granitoid areas that were eroding faster than the rest of the catchment. *Kober et al.* (2009) analysed different cosmogenic isotopes in the Lluta catchment in Chile (18.5^oS) and derived catchment-mean erosion rates between 0.01 and 0.05 mm/yr.

Time variations in these catchment-mean erosion rates were evidenced during the Late Pleistocene from the ^{10}Be analysis and luminescence dating of cut-and-fill terraces in the Piura, Pisco and Ocoña-Majes catchments (*Steffen et al.*, 2009, 2010; *Abbuehl et al.*, 2011b; *McPhillips et al.*, 2013; *Bekaddour et al.*, 2014). In an affluent of the Pisco River, *McPhillips et al.* (2013) ev-

idenced a decrease by a factor 2 between the Late Pleistocene and Holocene periods. *McPhillips et al.* (2014) measured ^{10}Be concentration in 70 individual cobbles in a 16 ka terrace and in the river bed and showed that cobbles are mainly derived from landslides, at a rate independent on climate. In the Ocoña catchment in Perú, ignimbrite dates, thermochronological studies, and numerical modelling of the river profile evolution were used to quantify the mean river incision rates over a longer time scale (Ma) (*Thouret et al.*, 2007; *Schildgen et al.*, 2007, 2009; *Jeffery et al.*, 2013). Since the last ∼16 Ma, the mean incision rate has varied between ∼0.03 and ∼0.15 mm/yr, values of the same order of magnitude as the Holocene estimates given by *Carretier et al.* (2015) in this catchment.

Local surface erosion rates were also obtained in this area, mostly in the most arid downslope part of the forearc. In southern Perú, *Hall et al.* (2008) used ^{10}Be to date surfaces at two sites (14.6^{o}S and 17.5^{o}S) as old as 1 Ma and to infer erosion rates between 0.04 and 0.3 mm/yr. Near 15.4^{o}S, *Saillard et al.* (2011) obtained ^{10}Be ages of Pleistocene marine terraces consistent with marine isotopic stages, suggesting a very low erosion rate of these terraces. In northern Chile (18.5^{o}S), *Kober et al.* (2007) combined ^{10}Be, ^{26}Al and ^{21}Ne concentrations at the surface of Mio-pliocene surfaces to calculate extremely low erosion rates ranging between 0.5 10^{-3} mm/yr and 2.25 10^{-3} mm/yr in the dryer part, and between 4 10^{-3} and 34 10^{-3} mm/yr at higher elevations under a wetter climate. Slightly more to the south (19.3^{o}S), *Dunai et al.* (2005) obtained Oligo-Miocene ages of sediment deposited on the highest desert surface close to the coast, implying negligible surface erosion rates.

Overall, these previous studies indicate local and catchment-mean erosion rates lower than 0.5 mm/yr with ranges spanning roughly two orders of magnitude.

Catchment lithologies

We selected seven rivers: Rio Cañete, Rio Ocoã, Rio Atico, Rio Grande, Rio Pisco, Rio Calientes (in Perú) and Rio Chiza (the only river in Chile). We gathered 16 sand samples at the foot of the main Cordillera (Figure 3). Above these samples, the catchment areas range between 536 (Rio Caplina) and 15,825 (Rio Ocoña) km^2 and their mean elevations range between 3,000 and 4,000 m. Catchment lithologies were obtained from the 1/1000000 Geological Map of Peru (Mapa Geolgico del Perú 1/1000000, Ingemmet, 1999, www.ingemmet.gob.pe/), and Chile (Mapa Geolgico del Chile 1/1000000, Sernageomin, 2002, www.sernageomin.cl/). In these seven catchments, the exposed rocks include Precambrian gneiss, Palaeozoic and Cretaceous granodiorites, Jurassic and Cretaceous continental sedimentary deposits, Oligo-Miocene to Plio-Pleistocene ingnimbrites and volcanoclastic deposits (mostly andesites and basalts but also ryolites) (Figure 3). These rocks have contrasting proportions of quartz, from granitoids that contain ∼25% of

quartz grains, to basalts and andesites that should not contain any quartz at all. We will later return to these assumptions in the discussion. The area covered by granitoids varies from 0 to 36%. Granitoids are spread out in several patches at different elevations in Rio Cañete and Rio Riplina, whereas they are concentrated at lower elevations in the catchments of Rio Pisco and Rio Ocoña. They are absent in the Rio Chiza catchment. For Rio Cañete and Rio Ocoña, we gathered samples along the main channel at sites located several tens of kilometres apart, which can be considered close given that the length of these rivers exceeds 200 km. Their ^{10}Be concentrations can be compared in order to study their variability over short distances. In Rio Grande, which is a braided river, we took two samples on two of the highest banks distance are 50 m apart and we treated them separately (GRA1 and GRA2).

Method

At each site, we sampled ∼2 kg of sand taken at different places located several metres apart in the river bed. The [0.5-1] mm fraction was processed. Samples were prepared at the Geosciences Environnement Toulouse (GET) ^{10}Be Laboratory or at the Cerege Laboratory following the protocol described in *von Blanckenburg et al.* (1996) and the ^{10}Be/ ^{9}Be ratio was obtained at the ASTER AMS in Cerege (France) and calibrated directly against the National Institute of Standards and Technology standard reference material 4325 by using an assigned value of (2.79±0.03).10E-11 (*Nishiizumi et al.*, 2007).

Mean catchment erosion rates were calculated based on the assumption that the ^{10}Be concentration has reached a steady state on the hillslopes, that this concentration did not change with river transportation, and neglecting the radioactive decay. All calculations involving topographic data used the SRTM digital elevation model with a pixel of ∼90 m. The ^{10}Be production rate due to spallation at each pixel was calculated using *Stone* (2000)'s production model, and a sea level production rate of 4.5 at g^{-1}. The muonic contributions used the sea level production rate from *Braucher et al.* (2003), scaled for elevation. At each pixel, an estimate of the topographic shielding coefficient between 0 and 1 was obtained using the method of *Codilean* (2006), which was multiplied by the previous total (neutron + muons) ^{10}Be production rate at each pixel. Then, the mean ^{10}Be production at the catchment scale was calculated following two approaches in order to calculate the weighted (ϵ_w) and unweighted (ϵ_u) erosion rates described in the theory section of this article.

In the first approach, the mean ^{10}Be production rate P_u was simply obtained by averaging the ^{10}Be production rates of the pixels, without differentiating between the different lithologies. Ignoring radioactive decay, the erosion rate ϵ_u was then obtained by $\epsilon_u = \sum_{i=1}^{3} \mu_i P_i / N$, where i denotes the neutrons, fast and stop muons, μ_i is the corresponding attenuation lengths taken from *Stone* (2000) (neutrons) and *Braucher et al.* (2003) (muons) and P_i is the associated

production rates. The considered rock density was 2.7 g/cm^3.

In the second approach, the ^{10}Be production rate of each pixel was additionally weighted by the relative proportion of quartz in the underlying lithology (P_w). This weighting follows the procedure of *Safran et al.* (2005) described by equation 10. The mean production rate P_w was obtained by averaging these weighted production rate values, leading to ϵ_w using the same equation as for ϵ_u.

For each lithology, we estimated the proportion of quartz minerals from the description of the 1/1000000 lithological maps. The estimated proportions of quartz are: granitoid rocks: 25%; rhyolites: 5%; undifferentiated detritic rocks: 5%; ignimbrites: 2%; and other volcanic rocks 0%. Possible errors on these values may affect P_w, an issue that we address in the discussion. In order to evaluate the largest bias that differences in the lithologies may cause, we also assumed that only granitoids contain quartz, as did *McPhillips et al.* (2013) for example in the Quebrada Veladera catchment, an affluent of the Rio Pisco (Figue 3). This is used to calculate a TCN production rate for granitoids only, P_g, and the corresponding erosion rate ϵ_g.

The uncertainty for the erosion rates ϵ_w and ϵ_u was calculated by propagating the analytical uncertainty for the ^{10}Be concentration measurements (1σ on the order of 3%) and we assumed 15% for the ^{10}Be production rate uncertainty.

Results

The ^{10}Be concentrations range between 81,000 at/g (OCO6) and 834,500 at/g (ATI1). For Rio Cañete Rio Ocoña, the geographically close samples show less than 20% of difference (Table 2). On the contrary, the ^{10}Be concentration for sample GRA1 from the Rio Grande is double that of sample GRA2, although these samples were taken approximately 50 m apart.

Erosion rates ϵ_u range between 0.02 and 0.4 mm/yr, i.e. the same range as obtained in previous studies in this region (Figure 4A). ϵ_u broadly increases with the catchment area. The largest ϵ_u is found in the largest Ocoña catchments.

However, ϵ_u is significantly higher than ϵ_w, weighted by quartz content, and ϵ_g, restricted to granitoids. This is illustrated by Figure 4, which shows the ratios of ϵ_u over ϵ_w and over ϵ_g (the ratio for the corresponding production rates are similar - Table 3). These ratios range between 1 to 2.5, showing that weighting by quartz content or limiting to granitoid yields lower erosion rate values. There is no relationship between these ratios and the proportion of catchment area underlaid by granitoids. The catchments with the largest ratios are those with granitoids mainly located in the lower half of the catchment, where slopes are the largest. These catchments are those of Rios Pisco, Grande and Ocoña. For the other catchments, there is no relationship between lithology

and elevation, and the ratio between ϵ_u and ϵ_w is smaller.

Discussion

TCN-derived erosion rates have been used to identify the main factors of millennial erosion along a mountain range. The effect of slope and slope threshold has been identified (e.g. *Binnie et al.*, 2007), whereas the effect of mean precipitation remains difficult to establish (e.g. *Carretier et al.*, 2013). In some cases, these classical erosion factors were not able to predict ^{10}Be-derived catchment erosion rates, with values that were apparently inconsistent with other observations (*Densmore et al.*, 2009). Part of the bias for the estimated erosion rates may be explained by stochastic processes that contradict the hypothesis outlined in Brown et al. and Granger et al. methods. For example, landslides in small catchments or incomplete mixing in the river may generate variations in the ^{10}Be concentration in river sediment, particularly in small catchments (*Niemi et al.*, 2005; *Binnie et al.*, 2006; *Reinhardt et al.*, 2007; *Yanites et al.*, 2009; *Savi et al.*, 2014). In large catchments (> 500 km^2) landslides should have less impact on the erosion rates (*Niemi et al.*, 2005; *Yanites et al.*, 2009), but on the other hand, the lithology may be more heterogeneous or the acquisition of ^{10}Be during river transport may be more significant (*Carretier et al.*, 2009). Two geographically close samples from the Rio Grande (one of the smallest catchments) gave different results, which may signify an incomplete mixing or a significant difference in the age of the sampled river banks. On the contrary, in the large rio Cañete and rio Ocoña catchments, the non-significant differences in the ^{10}Be concentration between relatively geographically close samples from the main channel suggest that the natural averaging of the river sediment is efficient.

The ratio between ϵ_w or ϵ_g and ϵ_u may reach a factor 2.5. The ϵ_u/ϵ_w ratio reaches 1.5, which is similar to the maximum value obtained for the theoretical catchments in Figure 1. The differences between ϵ_w, ϵ_g and ϵ_u are larger than the uncertainties for the ^{10}Be-derived erosion rates. Moreover, 10 of the 16 erosion rates ϵ_u differ by a factor of 2, between 0.05 and 0.1 mm/yr. Thus, lithological variations between catchments may add significant and different biases to these values. Note that we did not take the density variations of the parent rocks into account. These variations, potentially correlated with the quartz content, may also bias the calculated erosion rates if there is a relationship between rock density (lithology) and erosion rate, as shown in the Theory section. A particular case illustrating this issue deals with the concentration of quartz in the soil by chemical weathering of other minerals that dissolve faster. *Small et al.* (1999) and *Riebe and Granger* (2013) showed that the calculated denudation rate may be biased by a factor up to 2 if the change in the quartz content is not taken into account.

The largest $\epsilon_u/\epsilon_w \sim 1.5 - 2$ ratios (Rio Pisco, Rio Grande, Rio Ocoña) correspond to catchments where granitoids are located in the lowest half of the

catchments. These large values are consistent with the theoretical catchment discussed in the Theory section, for which a high quartz content is located at low elevations, and thus results in lower ^{10}Be production rates. Catchments with granitoid patches spread out at different elevations show smaller ϵ_u/ϵ_w ratios, even if they represent a small proportion of the catchment area.

Radioactive decay (neglected in our theoretical analysis and for the studied catchments) would probably increase the difference between ϵ_u and the true erosion rate ϵ. To illustrate this point, we can return to the bi-lithological example given in the introduction, in which we assume a catchment where a rock with low quartz content erodes quickly while a rock containing more quartz erodes slowly. The TCN concentration in the rapidly eroding rock is lower than in the slowly eroding rock. The radioactive decay increases this difference such that the amount of TCN from the rapidly eroding rock will be underestimated even more. Thus ϵ_u will also underestimate the true erosion rate. Nevertheless, the radioactive decay can significantly affect the results only if the sediment residence time on the hillslopes is comparable with the TCN half life, i.e. for catchment erosion rates less than ca. 10^{-3} mm/yr, which is not the case in the studied catchments. The relative contribution of muons and neutrons to the surface TCN production rate depends on the elevation. Thus if muons were included in the theoretical analysis, this would modify the ϵ_u/ϵ_w ratio by several percents only if the different lithologies are found at different elevations. Note that muons are taken into account in the calculation of ϵ_u/ϵ_w for the studied catchments.

It is beyond the scope of this paper to analyse the correlation between erosion rates and geomorphic parameters. Nevertheless, it is useful to analyse how the choice of calculating ϵ_u, ϵ_w or ϵ_g affects these correlations. We illustrate this by comparing these erosion rates with the catchment-mean slope, considered as one of the main erosion factors. A non-linear hillslope erosion model has been recently evidenced and seems robust over different tectonic, lithologic and climatic contexts (e.g. *Hanks*, 1999; *Roering et al.*, 1999; *Binnie et al.*, 2007; *Carretier et al.*, 2013; *Godard et al.*, 2014). This model is illustrated by the curves in Figure 5. In order to test if lithological variations are able to hamper the correlation of erosion rates with catchment-mean slope, we compare erosion rates ϵ_u, ϵ_w and ϵ_g with the model in Figure 5. ϵ_u does not fit well with this model. The fit is improved using ϵ_w. If we calculate the mean slope by weighting it by quartz content (Smean_w), then the fit between ϵ_w and Smean_w is significantly improved. Finally, the fit is much better when restricting the calculus to granitoids and comparing ϵ_g with Smean_g. Note that in the last case, the slope corresponds only to the mean granitoid slope Smean_g (Table 3). The improvement of the fit is due to both the change in erosion rate using ϵ_g, and to the selection of granitoid pixels to calculate the mean slope. This figure raises a question when a catchment includes rocks with a lot of quartz and other ones that are poor in this mineral, how should we treat this? Should we consider that all of the quartz comes from the quartz rich rock (as done

by *McPhillips et al.*, 2013), or should we consider that all lithologies should be included in the analysis because even a rock that has a low quartz content, but which is eroding fast, may significantly contribute to the quartz and ^{10}Be fluxes?

Figure 5 apparently suggests the first choice. Nevertheless, the apparent improved model fit using granitoids only does not necessarily support the choice of restraining the analysis to this rock. Other lithologies do contain quartz in a proportion that may be far from negligible, even for rocks mapped as having a lithology without quartz. For example, the Chiza catchment does not have any granitoids but quartz grains are still present in the sampled river sand. *Kober et al.* (2009) made the same observation in the Lluta catchment to the north of Chiza, where granitoids occupy only a small fraction of the catchment. Some ignimbrites in the Andes are dacites and contain phenocrystic quartz in a proportion greater than the several percents assumed from the 1:1000000 geological maps. Some carbonate or volcanic rocks may be silicified by processes following their formation. Although they may be interpreted as free from quartz using geological maps, they may significantly contribute to the quartz flux. For example, we observed that the Jurassic Caracoles formation, a carbonate formation of marine origin located in Antofagasta region (further to the south of the study area in this paper) is actually fully silicified. The same observation can be made locally with ignimbrites. Another example is the quartzic lithocap overlaying andesitic porphyries, common in this region of the Andes (e.g. *Sillitoe*, 2010). In practice, precise geological mapping allows these quartz sources to be identified. Nevertheless, information is not always available for large catchments. The best strategy should be to sample river sand from many subcatchments in order to avoid issues associated with lithological differences. This is not always possible. When sampling at the outlet of a large catchment with different lithologies, comparing P_u and P_w or ϵ_u and ϵ_w provides one way to estimate the possible "lithological" uncertainty, and to evaluate whether or not the correlation with geomorphic factors may be affected by this uncertainty (e.g. *Safran et al.*, 2005; *Carretier et al.*, 2013, 2014).

Conclusion

Weighting the TCN production rates by quartz content allows different quartz contents to be taken into account. Nevertheless, this approach may also bias the catchment-mean erosion rate if there is a spatial relationship between lithology and erosion rate. This type of relationship is not known a priori. In the case of the studied Central Andes catchments, the ϵ_u/ϵ_w ratio reaches a factor of up to 1.5-2. Calculating both ϵ_u and ϵ_w should help evaluate the uncertainty associated with contrasted lithologies and improve the correlation with geomorphic parameters.

Acknowledgments
This study was funded by the IRD, the French national research agency ANR

(project "ANDES" ANR-06-JCJC-0100). This paper is a contribution to LMI COPEDIM. S. Carretier would like to thank the Department of Geology at the University of Chile for its welcome. Sara Mullin corrected the english. We thank the Associated Editor and two anonymous reviewers for their constructive reviews.

References

Abbuehl, L. M., K. P. Norton, F. Schlunegger, O. Kracht, A. Aldahan, and G. Possnert (2010), El Nino forcing on ^{10}Be-based surface denudation rates in the northwestern Peruvian Andes? (vol 123, p 257, 2010), *Geomorphology*, *123*, 257–268, doi:10.1016/j.geomorph.2010.07.017.

Abbuehl, L. M., K. P. Norton, J. D. Jansen, F. Schlunegger, A. Aldahan, and G. Possnert (2011a), Erosion rates and mechanisms of knickzone retreat inferred from ^{10}Be measured across strong climate gradients on the northern and central Andes Western Escarpment, *Earth Surf. Proc. Land.*, *36*(11), 1464–1473, doi:10.1002/esp.2164.

Abbuehl, L. M., K. P. Norton, F. Schlunegger, O. Kracht, A. Aldahan, and G. Possnert (2011b), Corrigendum: El Nino forcing on ^{10}Be-based surface denudation rates in the northwestern Peruvian Andes? (vol 123, pg 257, 2010), *Geomorphology*, *129*(3-4), 417, doi:10.1016/j.geomorph.2011.02.023.

Aguilar, G., S. Carretier, V. Regard, R. Vassallo, R. Riquelme, and J. Martinod (2014), Grain size-dependent ^{10}Be concentrations in alluvial stream sediment of the Huasco Valley, a semi-arid Andes region, *Quaternary Geochronology*, *19*, 163–172, doi:http://dx.doi.org/10.1016/j.quageo.2013.01.011.

Barnes, J., and T. Ehlers (2009), End member models for Andean Plateau uplift, *Earth Planet. Sci. Lett.*, pp. 105–132, doi:10.1016/j.earscirev.2009.08.003.

Bekaddour, T., F. Schlunegger, H. Vogel, R. Delunel, K. Norton, N. Akçara, and P. Kubik (2014), Paleo erosion rates and climate shifts recorded by Quaternary cut-and-fill sequences in the Pisco valley, central Peru, *Earth Planet. Sci. Lett.*, *390*, 103–115.

Bierman, P. R., and E. J. Steig (1996), Estimating rates of denudation and sediment transport using cosmogenic isotope abundances in sediment, *Earth Surf. Proc. Land.*, *21*, 125–239.

Binnie, S., W. Phillips, M. Summerfield, and L. Fifield (2006), Sediment mixing and basin-wide cosmogenic nuclide analysis in rapidly eroding mountainous environments, *Quaternary Geochronology*, *1*, 4–14, doi:10.1016/j.quageo.2006.06.013.

Binnie, S. A., W. M. Phillips, M. A. Summerfield, and L. K. Fifield (2007), Tectonic uplift, threshold hillslopes, and denudation rates in a developing mountain range, *Geology*, *35*(8), 743–746.

Braucher, R., E. Brown, D. Bourlès, and F. Colin (2003), In situ produced ^{10}Be measurements at great depths: implications for production rates by fast muons, *Earth Planet. Sci. Lett.*, *211*, 251–258, doi:10.1016/S0012-821X(03)00205-X.

Brown, E. T., R. F. Stallard, M. C. Larsen, G. M. Raisebeck, and F. Yiou (1995), Denudation rates determined from the accumulation of in situ-produced ^{10}Be in the Luquillo Experimental Forest, Puerto Rico, *Earth Planet. Sci. Lett.*, *129*, 193–202.

Carretier, S., V. Regard, and C. Soual (2009), Theoretical cosmogenic nuclide concentration in river bedload clasts : Does it depend on clast size?, *Quaternary Geochronology*, *4*, 108–123, doi:10.1016/j.quageo.2008.11.004.

Carretier, S., V. Tolorza, M. Rodríguez, E. Pepin, G. Aguilar, V. Regard, J. Martinod, R. Riquelme, S. Bonnet, S. Brichau, G. Hérail, L. Pinto, M. Farías, R. Charrier, and J. Guyot (2014), Erosion in the Chilean Andes between 27S and 39S: Tectonic, climatic and geomorphic control, *The Geological Society London Special Publication*, *399*, doi:10.1144/SP399.16.

Carretier, S., V. Regard, R. Vassallo, G. Aguilar, J. Martinod, R. Riquelme, F. Christophoul, R. Charrier, and E. Gayer (2015), Differences in ^{10}Be concentrations between river sand, gravel and pebbles along the western side of the Central Andes, *Quaternary Geochronology*, *27*, 33–51.

Carretier, S., V. Regard, R. Vassallo, G. Aguilar, J. Martinod, R. Riquelme, E. Pepin, R. Charrier, G. Hérail, M. Farías, J.-L. Guyot, G. Vargas, and C. Lagane (2013), Slope and climate variability control of erosion in the Andes of central Chile, *Geology*, *41*(2), 195–198, doi:10.1130/G33735.1.

Codilean, A. (2006), Calculation of the cosmogenic nuclide production topographic shielding scaling factor for large areas using DEMs, *Earth Surf. Proc. Land.*, *31*(6), 785–794, doi:10.1002/esp.1336.

Densmore, A. L., R. Hetzel, S. Ivy-Ochs, W. Krugh, N. Dawers, and P. Kubik (2009), Spatial variations in catchment-averaged denudation rates from normal fault footwalls, *Geology*, *37*, F01,002, doi:10.1130/G30164A.1.

Dunai, T., G. Lopez, and J. Juez-Larre (2005), Oligocene-Miocene age of aridity in the Atacama Desert revealed by exposure dating of erosion-sensitive landforms, *Geology*, *33*(4), 321–324.

Farías, M., Charrier, D. Comte, J. Martinod, and G. Hérail (2005), Late Cenozoic deformation and uplift of the western flank of the Altiplano: Evidence from the depositional, tectonic, and geomorphologic evolution and shallow seismic activity (northern Chile at 19^{o}30S), *Tectonics*, *24*, TC4001, doi: 10.1029/2004TC001667.

Garcia, M., and G. Hérail (2005), Fault-related folding, drainage network evolution and valley incision during the Neogene in the Andean Precordillera of Northern Chile, *Geomorphology*, *65(3-4)*, 279–300, doi: 10.1016/j.geomorph.2004.09.007.

Garcia, M., R. Riquelme, M. Farías, G. Hérail, and R. Charrier (2011), Late Miocene-Holocene canyon incision in the western Altiplano, northern Chile: tectonic or climatic forcing?, *Journal of the Geological Society*, *168*(4), 1047–1060, doi:10.1144/0016-76492010-134.

Garreaud, R. D., M. Vuille, R. Compagnucci, and J. Marengo (2009), Present-day South American climate, *Palaeogeography Palaeoclimatology Palaeoecology*, *281*(3-4, Sp. Iss. SI), 180–195, doi:10.1016/j.palaeo.2007.10.032.

Garzione, C., P. Molnar, J. Libarkin, and B. Macfadden (2006), Rapid late Miocene rise of the Bolivian Altiplano: Evidence for removal of mantle lithosphere, *Earth Planet. Sci. Lett.*, *241*, 543–556.

Garzione, C., G. Hoke, J. Libarkin, S. Withers, B. MacFadden, J. Eiler, P. Ghosh, and A. Mulch (2008), Rises of the Andes, *Science*, *320*, 1304–1307.

Godard, V., D. L. Bourles, F. Spinabella, D. W. Burbank, B. Bookhagen, G. B. Fisher, A. Moulin, and L. Leanni (2014), Dominance of tectonics over climate in Himalayan denudation, *Geology*, *42*(3), 243–246, doi:10.1130/G35342.1.

Granger, D., , J. Kircher, and R. Finkel (1996), Spatially averaged long-term erosion rates measured from in situ-produced cosmogenic nuclides in alluvial sediment, *The Journal of Geology*, *104*, 249–257.

Hall, S. R., D. L. Farber, L. Audin, R. C. Finkel, and A. S. Meriaux (2008), Geochronology of pediment surfaces in southern Peru: Implications for Quaternary deformation of the Andean forearc, *Tectonophysics*, *459*(1-4), 186–205, doi:10.1016/j.tecto.2007.11.073, 6th International Symposium on Andean Geodynamics (ISAG), Barcelona, SPAIN, SEP 12-14, 2005.

Hanks, T. C. (1999), The age of scarplike landforms from diffusion-equation analysis, in *Quaternary geochronology: methods and applications, edited by J.S. noller, J.M. Sowers, and W.R. lettis*, pp. 313–338, AGU Washington DC.

Hippe, K., F. Kober, G. Zeilinger, S. Ivy-Ochs, C. Maden, L. Wacker, P. W. Kubik, and R. Wieler (2012), Quantifying denudation rates and sediment storage on the eastern Altiplano, Bolivia, using cosmogenic ^{10}Be, Al-26, and in situ C-14, *Geomorphology*, *179*, 58–70, doi:10.1016/j.geomorph.2012.07.031.

Hoke, G., B. Isacks, T. Jordan, N. Blanco, A. Tomlinson, and J. Ramezani (2007), Geomorphic evidence for the post-10 Ma uplift of the western fl ank of the central Andes, *Tectonics*, *26*, TC5021, doi:10.1029/2006TC002082.

Insel, N., T. A. Ehlers, M. Schaller, J. B. Barnes, S. Tawackoli, and C. J. Poulsen (2010), Spatial and temporal variability in denudation across the Bolivian Andes from multiple geochronometers, *Geomorphology*, *122*(1-2), 65–77, doi:10.1016/j.geomorph.2010.05.014.

Jeffery, M. L., T. A. Ehlers, B. J. Yanites, and C. J. Poulsen (2013), Quantifying the role of paleoclimate and Andean Plateau uplift on river incision, *J. Geophys. Res. Earth Surface*, *118*(2), 852–871, doi:10.1002/jgrf.20055.

Kober, F., S. Ivy-Ochs, F. Schlunegger, H. Baur, P. Kubik, and R. Wieleb (2007), Denudation rates and a topography-driven rainfall threshold in northern Chile: Multiple cosmogenic nuclide data and sediment yield budgets, *Geomorphology*, *83*, 97–120.

Kober, F., S. Ivy-Ochs, G. Zeilinger, F. Schlunegger, P. Kubik, H. Baur, and R. Wieler (2009), Complex multiple cosmogenic nuclide concentration and histories in the arid Rio Lluta catchment, northern Chile, *Earth Surf. Proc. Land.*, *34(3)*, 479–479, doi:10.1002/esp.1748.

McPhillips, D., P. R. Bierman, T. Crocker, and D. H. Rood (2013), Landscape response to Pleistocene-Holocene precipitation change in the Western Cordillera, Peru: ^{10}Be concentrations in modern sediments and terrace fills, *J. Geophys. Res. Earth Surface*, *118*(4), 2488–2499, doi:10.1002/2013JF002837.

McPhillips, D., P. R. Bierman, and D. H. Rood (2014), Millennial-scale record of landslides in the Andes consistent with earthquake trigger, *Nature Geoscience*, *7*, 925–930, doi:10.1038/NGEO2278.

Niemi, N., M. Oskin, D. Burbank, A. Heimsath, and E. Gabet (2005), Effects of bedrock landslides on cosmogenically determined erosion rates, *Earth Planet. Sci. Lett.*, *237*, 480–498, doi:10.1016/j.epsl.2005.07.009.

Nishiizumi, K., M. Imamura, M. Caffee, J. Southon, R. Finkel, and J. McAnich (2007), Absolute calibration of ^{10}Be AMS standards. Nuclear Instruments and Methods, *Physics Research*, *258*, 403–413.

Norton, K. P., F. von Blanckenburg, R. DiBiase, F. Schlunegger, and P. W. Kubik (2011), Cosmogenic ^{10}Be-derived denudation rates of the Eastern and Southern European Alps, *International J. of Earth Sciences*, *100*(5), 1163–1179, doi:10.1007/s00531-010-0626-y.

Reinhardt, L., T. Hoey, T. Barrows, T. Dempster, P. Bishop, and L. Fifield (2007), Interpreting erosion rates from cosmogenic radionuclide concentrations measured in rapidly eroding terrain, *Earth Surf. Process. Landforms*, *32*, 390–406, doi:10.1002/esp.1415.

Riebe, C., and D. Granger (2013), Quantifying effects of deep and near-surface chemical erosion on cosmogenic nuclides in soils, saprolite, and sediment, *Earth Surf. Proc. Land.*, *38(5)*, 523–533, doi:10.1002/esp.3339.

Roering, J. J., J. W. Kirchner, and W. E. Dietrich (1999), Evidence for nonlinear, diffusive sediment transport on hillslopes and implications for landscape morphology, *Wat. Resour. Res.*, *35*, 853–870.

Safran, E., P. Bierman, R. Aalto, T. Dunne, K. Whipple, and M. Caffee (2005), Erosion rates driven by channel network incision in the Bolivian Andes, *Earth Surf. Proc. Land.*, *30*, 1007–1024.

Saillard, M., S. R. Hall, L. Audin, D. L. Farber, V. Regard, and G. Herail (2011), Andean coastal uplift and active tectonics in southern Peru: ^{10}Be surface exposure dating of differentially uplifted marine terrace sequences (San Juan de Marcona, similar to 15.4 degrees S), *Geomorphology*, *128*(3-4), 178–190, doi:10.1016/j.geomorph.2011.01.004.

Savi, S., K. Norton, V. Picotti, F. Brardinoni, N. Akcar, P. Kubik, R. Delunel, and F. Schlunegger (2014), Effects of sediment mixing on 10Be concentrations in the Zielbach catchment, central-eastern Italian Alps, *Quaternary Geochronology*, *19*, 148–162.

Schaller, M., F. von Blanckenburg, N. Hovius, and P. Kubik (2001), Large-scale erosion rates from in situ-produced cosmogenic nuclides in european river sediments, *Earth Planet. Sci. Lett.*, *188*, 441–458, doi:ISI:000169449400011.

Schildgen, T., K. Hodges, K. Whipple, P. Reiners, and M. Pringle (2007), Uplift of the western margin of the Andean plateau revealed from canyon incision history, southern Peru, *Geology*, *35*, 523–526.

Schildgen, T., K. Hodges, K. Whipple, M. Pringle, M. van Soest, and K. Cornell (2009), Late Cenozoic structural and tectonic development of the western margin of the central Andean Plateau in southwest Peru , *Tectonics*, *28*, TC4007.

Schildgen, T., G. Balco, and D. Shuster (2010), Canyon incision and knickpoint propagation recorded by apatite 4He/3He thermochronometry, *Earth Planet. Sci. Lett.*, *293*, 377–387.

Sempere, T., A. Hartley, and P. Roperch (2006), Comment on Rapid uplift of the Altiplano revealed through 13C-18O bonds in paleosol carbonates, *Science*, *314*, doi:10.1126/science.113283.

Sillitoe, R. H. (2010), Porphyry Copper Systems, *Economic Geology*, *105*(1), 3–41.

Small, E., R. Anderson, and G. Hancock (1999), Estimates of the rate of regolith production using ^{10}be and al-26 from an alpine hillslope, *Geomorphology*, *27*, 131–150, doi:ISI:000078769000010.

Steffen, D., F. Schlunegger, and F. Preusser (2009), Drainage basin response to climate change in the Pisco valley, Peru, *Geology*, *37*, 491–494, doi: 10.1130/G25475A.1.

Steffen, D., F. Schlunegger, and F. Preusser (2010), Late Pleistocene fans and terraces in the Majes valley, southern Peru, and their relation to climatic variations, *Int J Earth Sci (Geol Rundsch)*, *99*, 1975–1989, doi:10.1007/s00531-009-0489-2.

Stone, J. (2000), Air pressure and cosmogenic isotope production, *J. Geophys. Res.*, *105*, 23,753–23,759, doi:ISI:000089895700027.

Thouret, J.-C., G. Worner, Y. Gunnell, B. Singer, X. Zhang, and T. Souriot (2007), Geochronologic and stratigraphic constraints on canyon incision and Miocene uplift of the Central Andes in Peru, *Earth Planet. Sci. Lett.*, *263*, 151–166.

von Blanckenburg, F. (2005), The control mechanisms of erosion and weathering at basin scale from cosmogenic nuclides in river sediment, *Earth Planet. Sci. Lett.*, *237*, 462–479.

von Blanckenburg, F., N. Belshaw, and R. O'Nions (1996), Separation of 9Be and cosmogenic ^{10}Be from environmental materials and SIMS isotope dilution analysis, *Chemical Geology*, *129*, 93–99.

Yanites, B., G. Tucker, and R. Anderson (2009), Numerical and analytical models of cosmogenic radionuclide dynamics in landslide-dominated drainage basins, *J. Geophys. Res.*, *114*, F01,007, doi:10.1029/2008JF001088.

Table 1: Definition of parameters.

ϵ_w	TCN derived erosion rate weighted by quartz content [L/T]
ϵ_u	TCN derived erosion rate unweighted by quartz content [L/T]
ϵ_g	TCN derived erosion rate considering granitoids only [L/T]
ϵ	True erosion rate [L/T]
N	TCN concentration in quartz [at/M of quartz]
P_w	TCN mean surface production rate weighted by quartz content [at/M of quartz/T]
P_u	TCN mean surface production rate unweighted by quartz content [at/M of quartz/T]
P	TCN surface production rate [at/M of quartz/T]
μ	Attenuation depth of particules [L]
ρ	Quartz density [M/L^3]
χ	Fraction of quartz in the parent rock [1]
Ψ_c	TCN outflux [at/T]
Ψ_q	Quartz outflux [M of quartz/T]
dx^2	Digital Elevation Model (DEM) Pixel area [L^2]
n	Number of pixels of catchment DEM
i	Denotes pixel "i"

Table 2: Data corresponding to ^{10}Be measurements from the Cerege ASTER AMS. Samples with "‡" are from *Carretier et al.* (2015). Samples with † were prepared at GET (Toulouse), the other ones at Cerege (Aix en Provence).

South Lat	South Long	Sample	Mass of Qz	^{9}Be	^{10}Be/^{9}Be	±	^{10}Be	±
^{o}	^{o}		g	at/g			at/g	
15.8906	73.1149	OCO1†	36.81	2.39E+019	1.24E-013	2.1E-014	8.10E+04	1.4E+04
15.9299	73.1192	OCO7	17.23	2.00E+019	1.49E-013	1.7E-014	1.73E+05	2.0E+04
16.1886	73.1561	OCO18†	37.21	2.39E+019	1.32E-013	8.7E-015	8.49E+04	6.1E+03
16.3476	73.1344	OCO22†‡	46.13	2.40E+019	1.91E-013	2.4E-014	9.95E+04	1.3E+04
16.1657	73.6311	ATI1	37.37	2.04E+019	1.53E-012	1.3E-010	8.34E+05	2.5E+04
14.5173	75.2108	GRA1†	36.89	2.39E+019	5.54E-013	2.7E-014	3.60E+05	2.0E+04
14.5173	75.2108	GRA2	13.5	1.99E+019	5.20E-013	2.8E-014	7.66E+05	5.0E+04
13.7343	75.9309	PIS2	28.27	1.96E+019	1.67E-013	2.1E-014	1.16E+05	1.5E+04
13.0275	76.1932	CAN2‡	24.18	1.95E+019	4.07E-013	2.5E-014	3.28E+05	2.1E+04
12.7766	75.9242	CAN5	24.03	2.00E+019	4.40E-013	2.4E-014	3.66E+05	2.0E+04
12.8306	75.9208	CAN8	27.21	1.96E+019	4.32E-013	2.3E-014	3.11E+05	1.8E+04
12.8000	12.8000	CAN10	16.49	1.98E+019	2.46E-013	1.8E-014	2.96E+05	2.2E+04
12.8000	12.8000	CAN12	15.04	1.97E+019	2.19E-013	3.0E-014	2.87E+05	4.2E+04
13.1247	76.3608	CAN17	17.77	2.09E+019	2.82E-013	2.4E-014	3.31E+05	2.9E+04
17.8500	70.1215	CAP1†	42.09	2.39E+019	6.97E-013	1.5E-013	3.96E+05	8.8E+04
19.1785	70.1561	CHIZ1	3.36	2.03E+019	2.05E-014	2.8E-015	1.17E+05	1.7E+04

Table 3: Results of the catchment analysis. A (km^2) is the area size. Hmean (m) is the mean elevation of the considered lithology. Smean (m/m) is the catchment-mean slope calculated using the 3 x 3 pixel slope average for the r.slope.ascpect command in GRASS. P is the ^{10}Be production rate. ϵ is the catchment-mean erosion rate. The subscript "$_w$" means that this value has been weighted by the quartz content, "$_u$" means that this value is unweighted by the quartz content, "$_g$" means that it is restricted to granitoids. Samples with "‡" are from *Carretier et al.* (2015).

Sample	A	Hmean	Smean	P_u	ϵ_u	±	P_w	ϵ_w	±	A_g	Hmean$_g$	Smean$_g$	P_g	ϵ_g	±
	km^2	m	m/m	at/g/a	mm/a		at/g/a	mm/a		km^2	m	m/m	at/g/a	mm/a	
OCO1	13972	4006	0.29	41.1	3.0E-01	7.E-02	28.7	2.1E-01	5.E-02	1441	2320	0.54	16.6	1.2E-01	3.E-02
OCO7	1061	2642	0.28	21.6	7.4E-02	1.E-02	13.9	4.7E-02	9.E-03	310	1827	0.39	11.9	4.1E-02	8.E-03
OCO18	15568	3838	0.29	38.9	2.7E-01	4.E-02	25.5	1.8E-01	3.E-02	1907	2139	0.51	15.0	1.0E-01	2.E-02
OCO22	15826	3786	0.29	38.2	2.3E-01	4.E-02	24.8	1.5E-01	3.E-02	1996	2079	0.5	14.6	8.6E-02	2.E-02
ATI1	1352	2194	0.24	15.1	1.1E-02	2.E-03	16.7	1.2E-02	2.E-03	485	2459	0.27	18.0	1.3E-02	2.E-03
GRA1	1855	3076	0.34	26.2	4.3E-02	7.E-03	17.7	2.9E-02	5.E-03	255	2033	0.48	13.7	2.2E-02	4.E-03
GRA2	1855	3076	0.34	26.2	2.0E-02	3.E-03	17.7	1.4E-02	2.E-03	255	2033	0.48	13.7	1.1E-02	2.E-03
PIS2	3699	3421	0.35	31.3	1.6E-01	3.E-02	18.7	9.5E-02	2.E-02	885	1958	0.45	13.1	6.6E-02	1.E-02
CAN2	5794	3777	0.44	36.1	6.5E-02	1.E-02	28.4	5.1E-02	8.E-03	1336	2825	0.49	24.0	4.3E-02	7.E-03
CAN5	3369	4244	0.43	42.3	6.8E-02	1.E-02	39.7	6.4E-02	1.E-02	478	3810	0.47	36.5	5.9E-02	9.E-03
CAN8	4319	4188	0.43	41.5	7.9E-02	1.E-02	37.9	7.2E-02	1.E-02	695	3687	0.49	34.5	6.5E-02	1.E-02
CAN10	5581	3872	0.44	37.2	7.4E-02	1.E-02	30.8	6.1E-02	1.E-02	1149	3091	0.5	26.7	5.3E-02	9.E-03
CAN12	5581	3872	0.44	37.2	7.6E-02	2.E-02	30.8	6.3E-02	1.E-02	1149	3091	0.5	26.7	5.5E-02	1.E-02
CAN17	6017	3657	0.43	35.0	6.2E-02	1.E-02	27.1	4.8E-02	8.E-03	1429	2693	0.48	22.8	4.1E-02	7.E-03
CAP1	537	3589	0.36	35.0	5.2E-02	1.E-02	30.4	4.5E-02	1.E-02	74	3323	0.39	29.1	4.3E-02	1.E-02
CHIZ1	2236	2049	0.21	15.3	8.7E-02	2.E-02	11.1	6.0E-02	1.E-02						

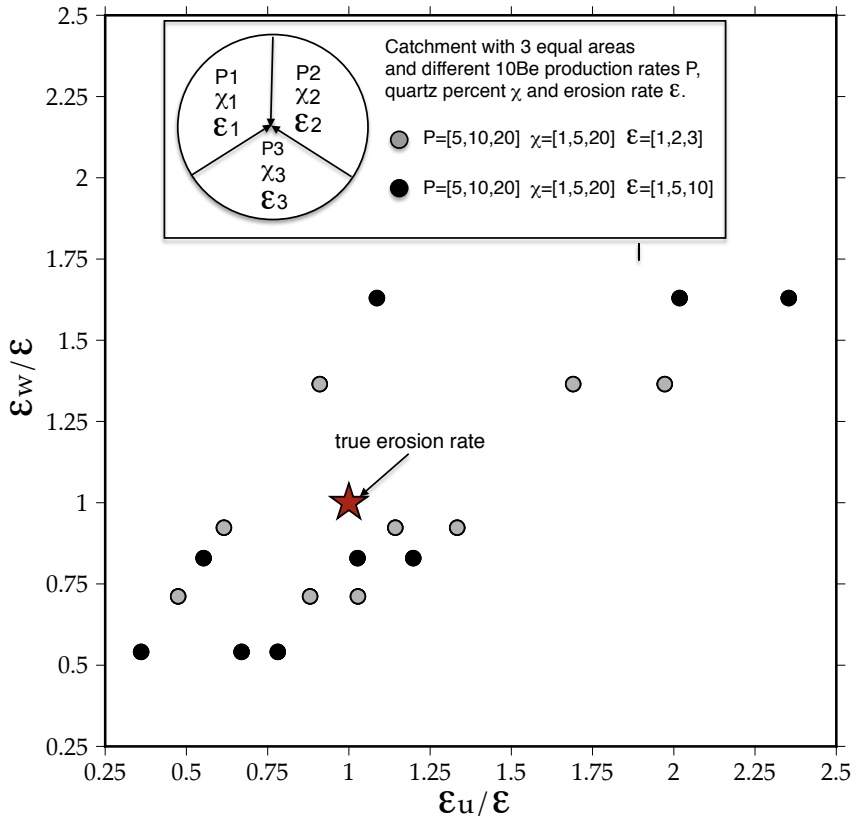

Figure 1: Bias generated by calculating ϵ_u (unweighted by the lithology) and ϵ_w (taking lithology into account). ϵ is the true catchment-mean erosion rate. Values are non-dimensional. A theoretical catchment includes three different lithologies (thus different quartz proportions χ_i) spread out into equal areas, at three different elevations (thus different ^{10}Be production rates P_i), and eroding at three different rates ϵ_i. By varying P_i, χ_i and ϵ_i according to the values given in the graph, different values of ϵ_u (Equations 1 and 12) and ϵ_w (Equation 11) are calculated and divided by ϵ.

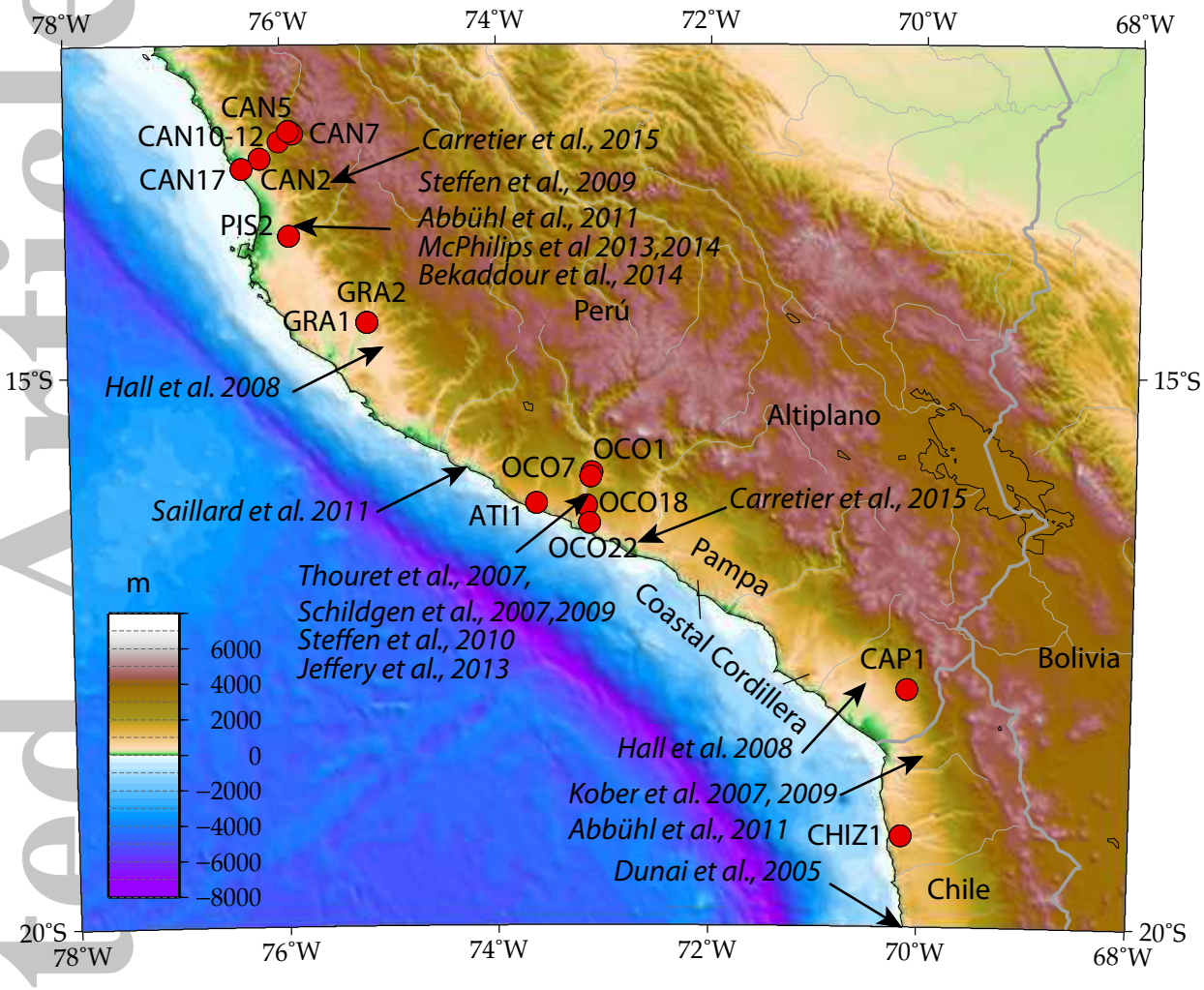

Figure 2: Situation map with locations of the samples. The references are previous works on erosion in this area.

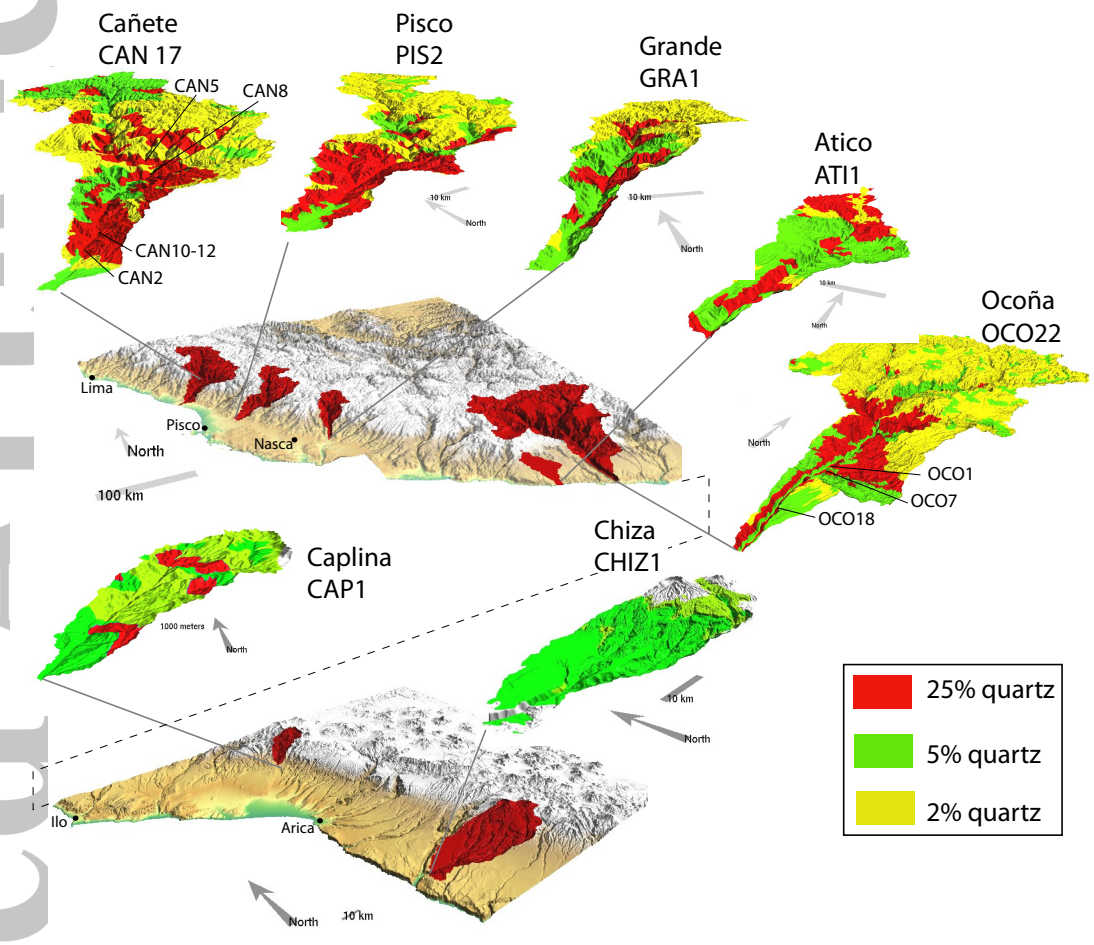

Figure 3: Catchments with their proportion of quartz deduced from the 1/1000000 geological maps of Perú and Chile.

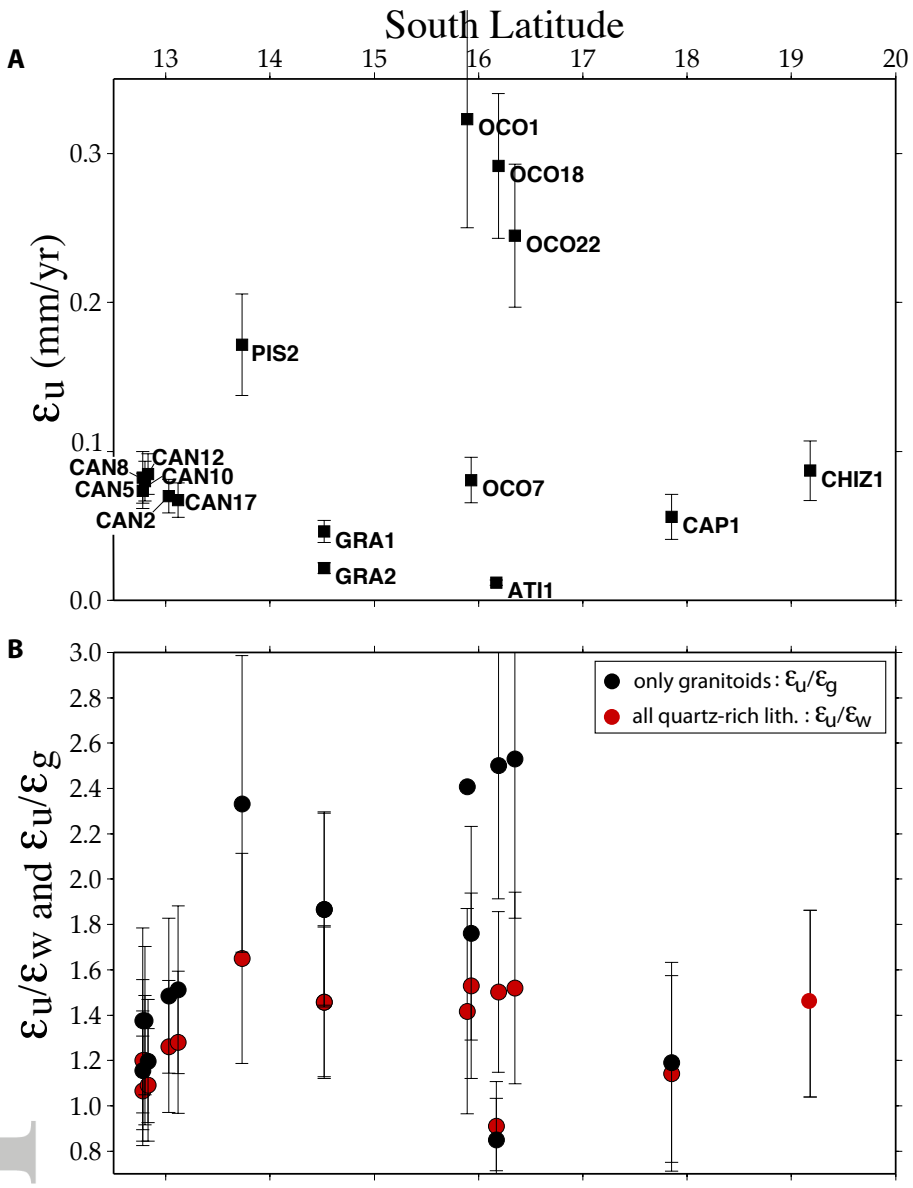

Figure 4: (A)- Erosion rates derived from the ^{10}Be concentration in river sand without correcting the ^{10}Be production rate by quartz content. Error bars include the analytical uncertainties of the ^{10}Be concentrations and 15% of uncertainty for the ^{10}Be production rates. (B) Latitudinal variations in the catchment-mean erosion rates ϵ_u over ϵ_w and ϵ_g. The red circles take all quartz-rich lithologies into account, whereas the black points only consider the granitoids. Uncertainties were obtained by $(\epsilon_u/\epsilon_w)\sqrt{((\sigma\epsilon_u/\epsilon_u)^2 + (\sigma\epsilon_w/\epsilon_w)^2)}$ where σ is the 1 σ uncertainty.

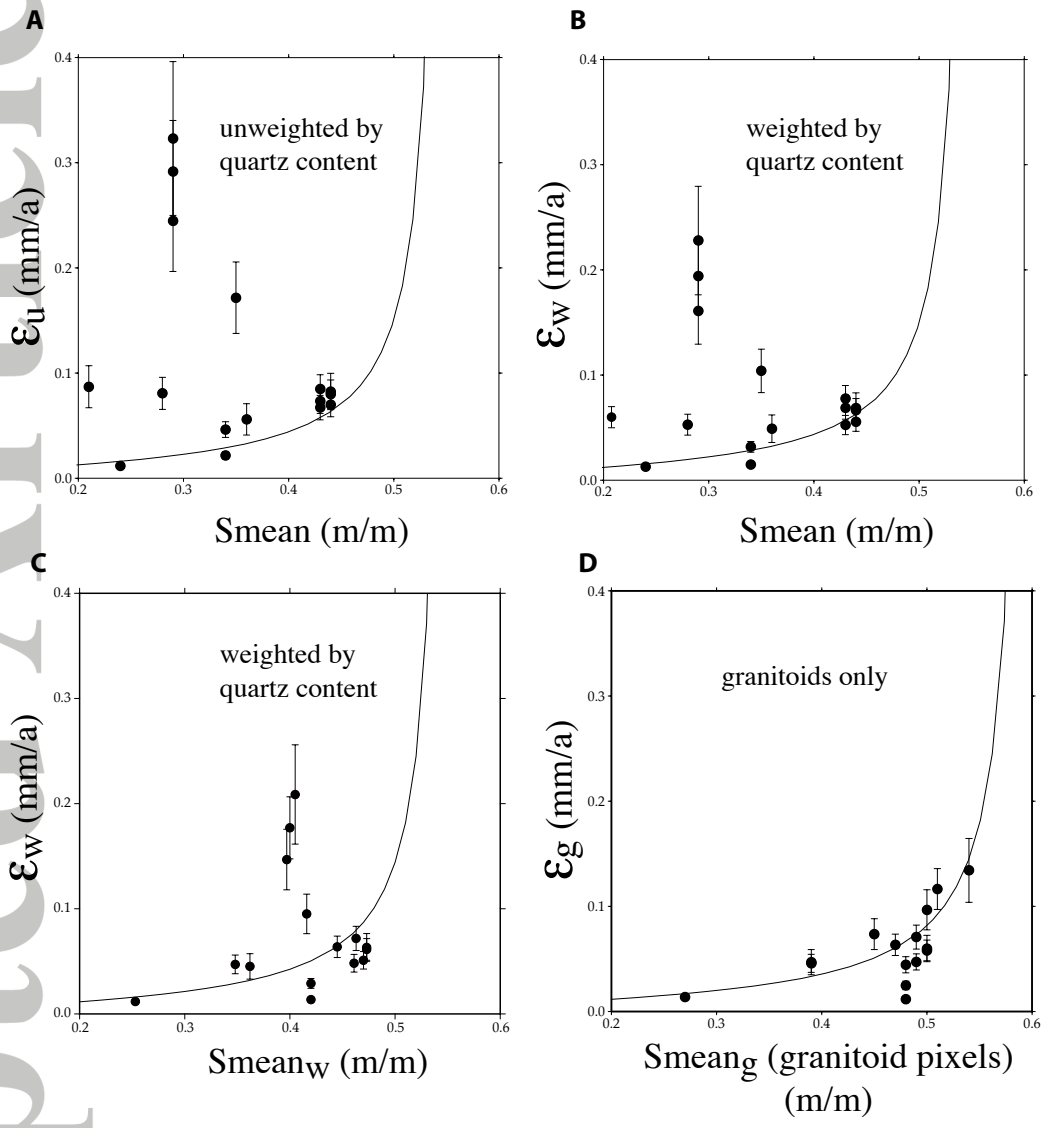

Figure 5: Catchment-mean erosion rate versus 3 x 3 slope (calculated using the SRTM dem). (A) The erosion rate ϵ_u is calculated without taking differences in the quartz content in quartz-rich lithologies into account. (B) The erosion rate ϵ_w is weighted by the quartz content. (C) The same as (B) but the mean slope is calculated by weighing local slopes by the quartz content. (D) The erosion rate ϵ_g is calculated by assuming that only granitoids provide quartz to the river channel. The mean slope is also calculated for granitoids only. The solid line is a model of the form $\epsilon = \kappa \frac{S}{1-(S/S_c)^2}$, where K is a transport coefficient, S is the slope, $S_c = 0.55$ in (A) and (B), and $S_c = 0.6$ in (C) (e.g. *Roering et al.*, 1999).